Article:
Vukicevic, AM, Zelic, K, Milasinovic, D et al. (6 more authors) (2021) OpenMandible: An open-source framework for highly realistic numerical modelling of lower mandible physiology. Dental Materials, 37 (4). pp. 612-624. ISSN 0109-5641

https://doi.org/10.1016/j.dental.2021.01.009

OpenMandible: An open-source framework for highly realistic numerical modelling of lower mandible physiology

Arso M. Vukicevic*[,1], Ksenija Zelic[2], Danko Milasinovic[3], Ali Sarrami-Foroushani[4], Gordana Jovicic[1],
Petar Milovanovic[2], Marija Djuric[2], Nenad Filipovic[1], Alejandro F. Frangi[4,5]

[1]Faculty of engineering, University of Kragujevac, Kragujevac, Serbia
[2]Laboratory for Anthropology, Institute of Anatomy, School of Medicine, University of Belgrade, Belgrade, Serbia
[3]Faculty of Hotel Management and Tourism in Vrnjačka Banja, University of Kragujevac
[4]Centre for Computational Imaging and Simulation Technologies in Biomedicine (CISTIB), School of Computing and School of Medicine, University of Leeds, Leeds, UK; Leeds Institute of Cardiovascular and Metabolic Medicine, School of Medicine, University of Leeds, Leeds, UK;
[5]Medical Imaging Research Center (MIRC), University Hospital Gasthuisberg. Cardiovascular Sciences and Electrical Engineering Departments, KU Leuven, Leuven, Belgium.
*Corresponding author {arso_kg@yahoo.com; +381643483552; Sestre Janjic 6, 34000 Kragujevac, Serbia}

Abstract

Objective: Computer modeling of lower mandible physiology remains challenging because prescribing realistic material characteristics and boundary conditions from medical scans requires advanced equipment and skill sets. The objective of this study is to provide a framework that could reduce simplifications made and inconsistency (in terms of geometry, materials, and boundary conditions) among further studies on the topic.

Methods: The OpenMandible framework offers: 1) the first publicly available multiscale model of the mandible developed by combining cone beam computerized tomography (CBCT) and μCT imaging modalities, and 2) a C++ software tool for the generation of simulation-ready models (tet4 and hex8 elements). In addition to the application of conventional (Neumann and Dirichlet) boundary conditions, OpenMandible introduces a novel geodesic wave propagation approach for incorporating orthotropic micromechanical characteristics of cortical bone, and a unique algorithm for modeling muscles as uniformly directed vectors. The base intact model includes the mandible (spongy and compact bone), 14 teeth (comprising dentin, enamel, periodontal ligament, and pulp), simplified temporomandibular joints, and masticatory muscles (masseter, temporalis, medial, and lateral pterygoid).

Results: The complete source code, executables, showcases, and sample data are freely available on the public repository: https://github.com/ArsoVukicevic/OpenMandible. It has been demonstrated that by slightly editing the baseline model, one can study different "virtual" treatments or diseases, including tooth restoration, placement of implants, mandible bone degradation, and others.

Significance: OpenMandible eases the community to undertake a broad range of studies on the topic, while increasing their consistency and reproducibility. At the same time, the needs for dedicated equipment and skills for developing realistic simulation models are significantly reduced.

Keywords: OpenMandible, mandible, simulation, dentistry, open source.

1 Introduction

With progress in computer science and the understanding of human physiology, there is a growing trend of using computer simulations to analyze and predict the response of biomaterials under physiological loadings [1]. The significant benefits that numerical (or *in silico*) studies have brought to biomedical science and industry include reduced cost, time, and effort necessary for performing traditional (*in vivo*) experiments. *In silico* studies are often the only non-invasive method of estimating a patient's response to physiologic loads, medical devices, or drugs. Compared to traditional experiments, computer simulations avoid deterioration of the mandible and allow varying acting forces and material properties. Furthermore, simulation provides information about the physical response (i.e., stress and strain distribution) throughout the model that cannot be measured experimentally [2]. A series of simulation models that differ only in one property or condition can be generated to investigate how the variations influence the biomechanical response of a tooth (or human physiology in general)[1] [3].

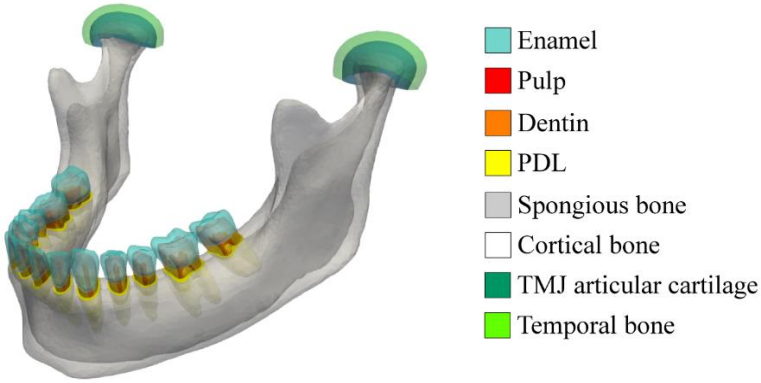

Fig. 1 – Open Mandible base (intact) model with its accompanying constitutive materials.

This study focuses primarily on the stomatology domain, or more precisely, on the numerical modeling of the lower jaw or mandible [4, 5]. A model of the intact mandible should include these materials (Fig. 1): bone (cortical and trabecular), teeth (with corresponding materials: enamel, dentine, and pulp), periodontal ligament (PDL), and temporomandibular joints, together with accompanying masticatory muscles (see Fig. 6). In practice, the development of realistic mandible models is challenging for several reasons. First, the dimensions of masticatory and dental tissues are at different

[1] International regulatory bodies have recently recognized these benefits and have begun incorporating numerical simulations into industry standards as a prerequisite for obtaining FDA approval for novel medical devices, drugs, and treatments.

scales, and difficult to reconstruct using conventional imaging modalities (the thickness of enamel and PDL are on edge with slice-thickness of CT/CBCT devices). Moreover, a considerable segment of the dentistry community focuses on artificial restorative materials (metals, ceramics), which produce echoes in medical scans and aggravate reconstruction [6]. Materials used to replace damaged parts of a tooth (dental fillings, crowns, dental posts) or replace teeth (dental implants and fixed or removable prostheses) are typical examples. As a solution, restorations are commonly studied using virtual models, obtained by modifying reconstructions of intact mandibles.

Accurate 3-D modeling of the complete lower mandible is a challenging and time-consuming[2] process. To date, there have been several initiatives aimed at developing virtual models of human physiology with a valuable impact in clinical and industrial applications. The pioneer attempt was the Visible Human Project (VHP), which provided CT and MRI images obtained from one male and one female cadaver [7]. Since 1995, over 4,000 licenses (from 66 countries) have been granted to researchers issuing access to the VHP datasets (since 2019, a license is no longer required). However, in one study using VHP data, the authors could not reconstruct anatomically complete mandibles (with all teeth and their constituent materials) [8]. Studies have used the virtual Chinese human (VCH) with similar obstacles [9]. The virtual population (ViP) is a commercial set of whole-body anatomical models created from magnetic resonance scans [10]. Although ViP models are widely used for *in silico* studies of electromagnetic compatibility, they do not differentiate between multiple tooth tissues[3]; they are oversimplified for dental applications. Although one may find models of a single tooth with surrounding tissues [11], a detailed model of the complete mandible with all corresponding materials and boundary conditions (BCs) is not available to the scientific community. The complexity of developing models and BCs has significantly increased in the last few years; most of the scientific community faces difficulties in reproducing them in commercial and in-house simulation software packages. Public unavailability and model inconsistency (in terms of geometry, materials, and BCs) in previous studies make objective comparison of findings difficult.

The aim of this study is to 1) develop a detailed model of the lower jaw (with all material characteristics and physiological conditions of interest), and 2) create a user-friendly C++ software framework to encourage use by the broader community. OpenMandible intends to support further studies by providing a public model that is easily adaptable to different user scenarios. The remaining sections of this paper are organized to answer three key questions of interest to the community: 1) What are the best practice requirements from the literature? 2) How are these features algorithmically implemented within the proposed framework? 3) How should these features be used to efficiently

[2] To illustrate the required effort, the extraction of the baseline intact OpenMandible model from medical scans required three months and highly dedicated equipment and expertise not widely available to our community.

[3] https://itis.swiss/assets/Downloads/VirtualPopulation/Tissue-list-V4.0/Yoon-sun-V4.0-tissuelist.txt

simulate lower mandible-related problems? These three areas were covered to ensure development of physiologically accurate and consistent simulation models using the provided framework.

2. Materials and methods

2.1 Development of the baseline model from clinical and preclinical imaging

The OpenMandible baseline model was developed from a dry, well-preserved, male skull from an osteological collection of the Laboratory for Anthropology, Institute of Anatomy, School of Medicine, University of Belgrade, Serbia. The mandible was scanned using cone beam computerized tomography (CBCT). Imaging was performed using a high-resolution CBCT device (SCANORA 3Dx, SOREDEX, Tuusula, Finland; 0.133 mm pixel spacing, 0.133 mm slice thickness). The skull was scanned using computerized tomography (Siemens Somatom Sensation 16, Munich, Germany), as it was too large for CBCT scanning. Resolving the skull was not critical, as it was used only to estimate muscle force directions. The PDL is only ~0.2 mm thick; with pulp and enamel, it cannot be accurately reconstructed from conventional CT and CBCT scanners (slice thicknesses 0.1~0.4 mm). To achieve better scanning resolution for teeth materials, all mandibular teeth were carefully removed from the jaw and scanned using micro-computed tomography (μCT). Each tooth was attached to a standard sample holder and examined using a high-resolution μCT system (SkyScan μCT 1172, Bruker, Belgium) at a nominal resolution of 10 μm. The obtained images were reconstructed using NRecon software (Bruker, Belgium) and saved as DICOM files.

After obtaining DICOM files, segmentation and reconstruction of the corresponding surface meshes were performed using Mimics 10.01 (Materialize, Leuven, Belgium). The process included semi-automatic image thresholding and annotation to ensure accurate segmentation of materials in each DICOM slice. Experienced dentists were responsible for annotating tissues/materials in 2-D planes. The software reconstructed 3-D triangulated surfaces (using the 'marching cubes' algorithm) from annotated 2-D slices. Separate STL surface meshes were generated for each material of interest, as shown in Fig. 2(b).

In most cases, the quality of a mesh retrieved directly from the Mimics software (or any surface reconstruction) is not suitable for performing simulations. We were unable to ideally segment each DICOM slice, which negatively affected the algorithm reconstructing the surface mesh from the segmented slices[4]. Additional surface mesh refinement and assembly of different model components were performed in the Geomagic Studio 10 mesh editor (Geomagic GmbH, Stuttgart, Germany). We used different features for manipulation of triangular surface meshes, which enabled us to repair low-

[4] At this stage, the size of one triangle (composing blocks of the mesh) is determined with the resolution of a CBCT or μCT scanner, which is often not proportional to the dimensions of dental tissues. As a consequence, the mesh does not contain the optimal number of triangles needed to describe the surface of teeth. More important, many of the triangles are of low quality (sharp edges), which negatively affects the accuracy of the numerical analysis.

quality elements and cut, merge, or smooth the regions of interest. We ensured that each contact surface between the two materials shared[5] nodes/triangles.

2.2 Workflow and architecture of the proposed framework

The OpenMandible framework was developed to be generic and cross-platform, independent of PC operating systems, software tools used for mesh editing, and user-chosen numerical solvers or simulation packages. We adopted stereolithography (STL) as the input file format, as it is a widely accepted format for representing surface meshes in any CAD software (MeshLab, 3DSlicer, Geomagic, Materialise Mimics, etc.). The architecture and modules of the proposed OpenMandible framework are shown in Fig. 2(c). We emphasize that the framework was developed on top of dfemtoolz, a highly efficient C++ open-source library for imposing BCs in biomedical simulations [12]. It was adapted and extended with features for meshing multi-material mandible models and prescribing different types of BCs from input STL files. The software outputs were written as plain text *.txt files (and *.vtk and *.pos data for visualization purposes), which contain all information regarding the generated model and prescribed BCs. Thus, we assume that the user can import (copy) the generated data from the output files into a format appropriate for his/her solver of choice (Abaqus, ANSYS, Elmer, or an in-house solver)[6].

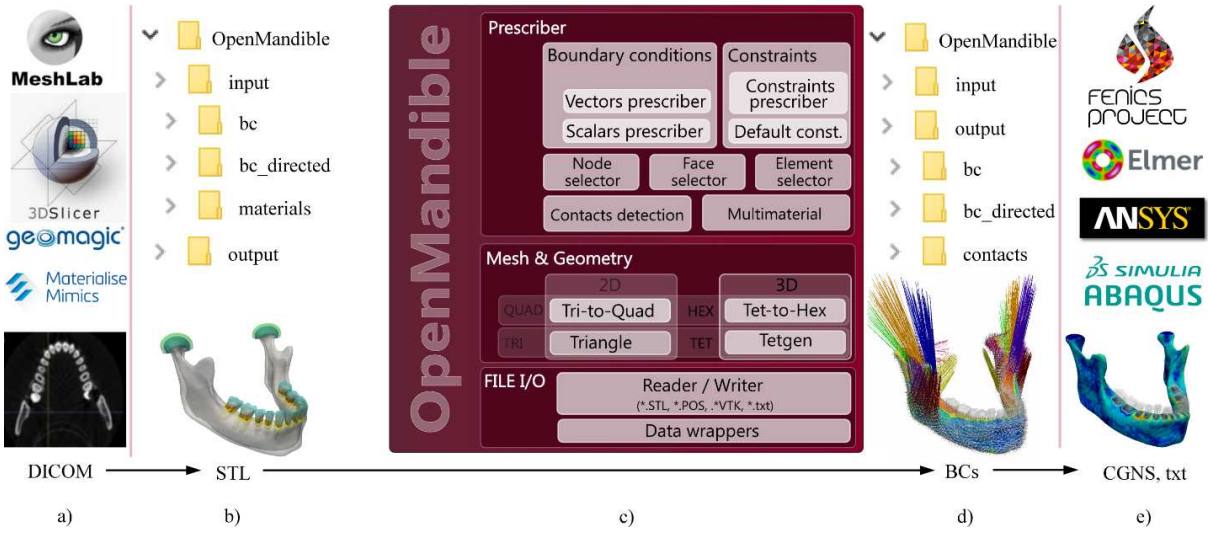

Fig. 2 – Workflow and architecture of OpenMandible: a) Extraction of surface meshes of dental tissues from corresponding medical scans; b) Structure of OpenMandible input folders; c) OpenMandible architecture; d) OpenMandible output folders; e) Importing model into simulation packages and running simulations.

[5] Otherwise, we are not able to model/assemble a tooth (composed of different materials), except as a series of disconnected parts.

[6] To demonstrate this, we set up an exemplar simulation in ANSYS Transient Structural by importing the mesh, material properties, and BCs generated in OpenMandible.

2.3 Organisation of model inputs and outputs

Each material and boundary condition should be defined with a separate STL file, and saved into the input folders (see Fig. 2b top). Thus, users can use the framework with any conventional CAD software for mesh pre-processing and manipulation[7]. The "input" folder has three subfolders: 1) materials, 2) bc, and 3) bc_directed; and two files: aOsteonsFile.txt and open_mandible_program_parameters.cfg, for prescribing the cortical bone orthotropy and configuring the program execution, respectively (see Section 2.4). The "materials/stl" folder contains STL surface meshes for each part/material (cortical bone, cancellous bone, teeth, implants, etc.). By default, there are 60 STL files; a user may include/exclude any material at will (use-cases are provided in the Discussion section and Appendix A). The folder "bc" contains STL files (that define nodes/surfaces) where constraints or loads must be prescribed. Similarly, the "bc_directed" folder contains STL pairs for prescribing muscles as directed forces/vectors.

2.4 The OpenMandible Commands

All instructions for generation of mandible models and BCs are contained in the config file (open_mandible_program_parameters.cfg), which is split into six blocks/sections. In this file, a user must set:

- Section A: Element type (supported types of elements are tet4/hex8).
- Section B: The list of materials (from the folder input/materials) to be discretized into volumetric meshes.
- Section C: The list of nodal and surface BCs (for prescribing constraints, scalars, and vectors that act perpendicularly to the selected surface).
- Section D: The list of directed nodal BCs (used for defining muscles, forces, and others).
- Section E: Cortical bone orthotropy settings.
- Section F: Output file formats (*.txt, *.pos, and *.vtk are supported).

For sections C and D, the adopted command format is: "material filename1.stl filename2.stl intensity" (Fig. 3). The "material" string determines the material on which BCs are applied (i.e. cortical bone, or enamel); "filename1.stl" points to the STL file with nodes/faces to be selected from the material; "filename2.stl" points to the STL file that contains a surface/nodes that should be used for computing the direction of the prescribed loads. The final parameter determines the direction and

[7] This implies that a minimum of three nodes can be selected - considering the size of the elements and model (millions of nodes), we found this is an appropriate approach. However, if one wants to prescribe BC on a single node, it can easily be done by neglecting two overabundant nodes, or by making changes in the source-code (which is provided along with this manuscript).

intensity of the prescribed loads (1 outward and -1 indicates direction outward, but any decimal number can be used to define vector magnitudes).

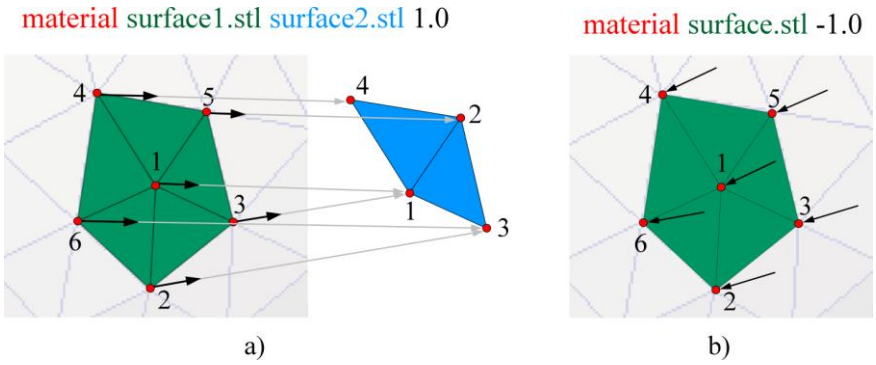

Fig. 3 – Sketch of OpenMandible commands for prescribing BCs: a) Format of commands for prescribing directed BCs (muscles, forces, springs); b) Format of commands for prescribing BCs on/normal to surfaces (constraints, pressure, forces). The green surface is the input *.stl file defining the model surface where BCs should be specified. The blue surface is the input *.stl file used for determining the directions of prescribed vectors.

3 OpenMandible features for developing state of the art simulation models of mandible physiology

In this section, we review the best practices from the literature, with an emphasis on how they can be reproduced using the OpenMandible framework.

3.1 Modelling of cortical and cancellous bone

Although the mandible is the largest and strongest bone of the facial skeleton, its injuries are among the most frequent facial bone injuries [13–15]. Additionally, the mandible is the supporting bone for both teeth and implanted materials. Thus, realistic modeling of its components (cortical and cancellous bone) is essential for obtaining reliable computer simulation results. Although the cortical bone has been frequently modeled as a homogeneous material, experiments have shown that the mandibular tissue behaves as an anisotropic material; its strength depends on the orientation of osteons to the direction of a load [16, 17]. The lack of realism in the literature may be justified by the technical difficulty of applying anisotropic material across the complex geometry of the mandible. OpenMandible solves this problem with a dedicated algorithm for incorporating the micromechanical properties of the mandibular cortex, splitting the mandible into 16 anatomical zones (facial and lingual), as shown in Fig. 4 [18]. The material properties for each zone of the facial and lingual cortical bone are presented in Table 1.

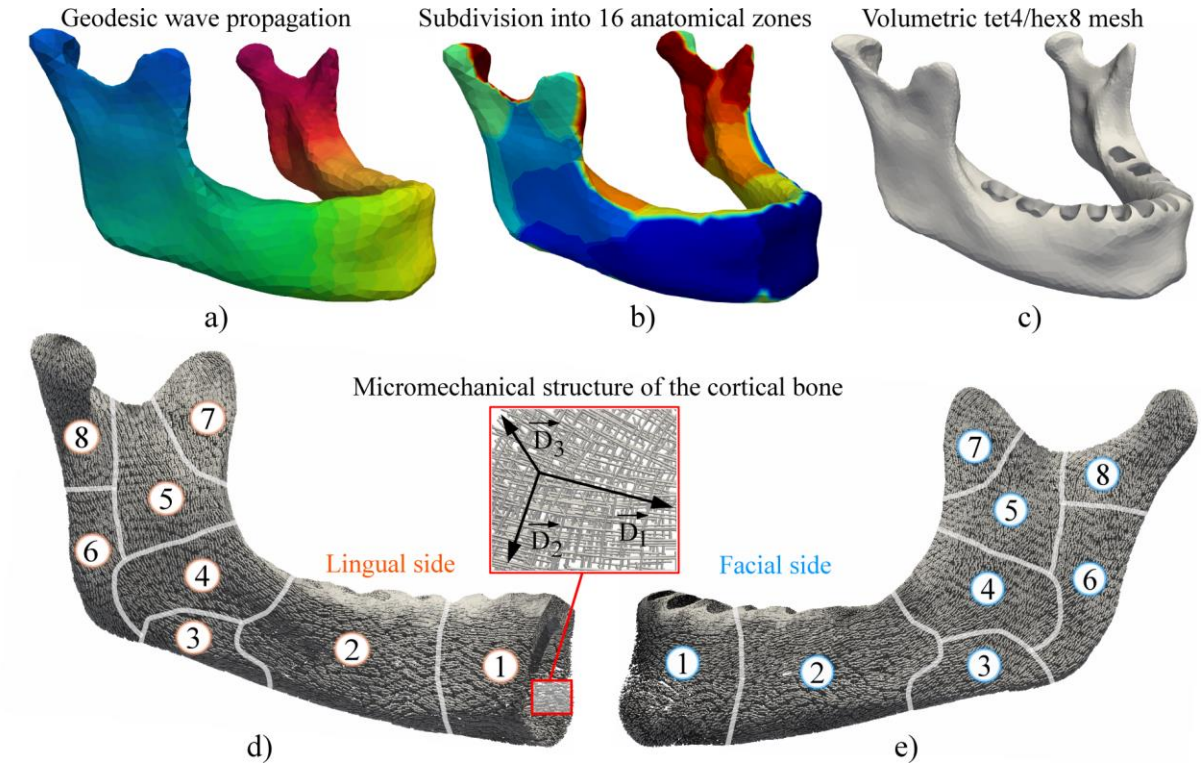

Fig. 4 – Application of orthotropic micro-material characteristics on the lower mandible: a) Geodesic wave propagation; b) Subdivision of simplified cortical bone mesh into 16 anatomical zones; c) Detailed volumetric mesh of the cortical bone; d) and e) Resulting osteon directions (with focus on the micromechanical structure of the developed osteons).

Table 1. Mechanical characteristics of orthotropic zones of facial (F) and lingual (L) cortical bone: Elastic moduli (E), Poisson's ratios (ν), and shear moduli (G) in GPa for the human dentate mandible. The numbers are given in the subscript (e.g. $E_{1,}$ $\nu_{12,}$ G_{12}) are related to the orthotropy and indicate the directions of the three orthogonal axes: D_1, D_2, and D_3; 〉 is Density [18, 19].

Zone	E_1 10^3 MPa	E_2 10^3 MPa	E_3 10^3 MPa	$\nu_{12}=\nu_{21}$ -	$\nu_{13}=\nu_{31}$ -	$\nu_{23}=\nu_{32}$ -	$G_{12}=G_{21}$ 10^3 MPa	$G_{13}=G_{31}$ 10^3 MPa	$G_{23}=G_{32}$ 10^3 MPa	〉 [kg/m³]
1F	11.51	15.38	20.00	0.20	0.41	0.33	4.57	4.98	6.57	1810
2F	12.98	18.03	23.22	0.22	0.428	0.32	5.10	5.65	7.67	1970
3F	11.35	18.05	20.10	0.15	0.48	0.34	4.70	5.10	7.25	1940
4F	14.15	20.15	28.15	0.27	0.34	0.27	5.15	5.80	8.05	1990
5F	12.55	19.27	22.40	0.19	0.46	0.32	5.10	5.55	7.70	1970
6F	13.60	18.10	26.10	0.26	0.37	0.28	5.10	5.50	7.60	1960
7F	14.00	19.55	28.55	0.27	0.325	0.325	5.20	5.75	7.65	2000
8F	13.20	18.00	25.95	0.26	0.37	0.265	5.05	5.55	7.45	1940
1L	12.78	17.31	20.98	0.21	0.45	0.34	5.08	5.65	7.25	1930
2L	12.46	17.69	20.31	0.19	0.46	0.35	5.07	5.39	7.25	1930
3L	12.65	19.40	22.60	0.20	0.445	0.32	5.05	5.45	7.75	1980
4L	12.65	19.20	26.55	0.21	0.39	0.297	5.02	5.40	7.20	1940
5L	12.64	18.02	23.02	0.26	0.32	0.26	4.80	5.10	6.85	1930

6L	12.70	17.35	24.55	0.25	0.34	0.235	4.75	5.50	7.40	1870
7L	13.25	17.25	25.50	0.24	0.32	0.25	5.20	5.40	7.10	1900
8L	12.65	17.75	24.50	0.21	0.40	0.30	5.05	5.15	7.30	1950

1F(L) = Symphysis (basis + pars alveolaris); 2F(L) = Body (basis + pars alveolaris); 3F(L) = Angle (inferior part); 4F(L) = Angle (superior and middle part); 5F(L) = Ramus (middle and frontal part); 6F(L) = Posterior ramus and a part of inferior border of the angle region; 7F(L) = Coronoid process; 8F(L) = Condylar process.

The principal axes needed for modeling cortical bone orthotropy were determined using wave propagation (Fig. 4). Starting from the right condyle, a wave was propagated over the outer surface of the simplified surface mesh of the cortical bone if the gradients of the wavefront corresponded to the directions of the osteons (Fig. 4a). To ensure equal and smooth propagation from the source points, the front propagation was controlled with the geodesic distance. In the literature, the problem of determining orthotropy axes was recently solved by modeling the osteonal orientations as harmonics fields [20, 21]. In this study, we avoided the use of simulation software for the development of mandible BCs. Moreover, we assigned appropriate anatomical zone IDs to each node of the simplified surface mesh (Table 1, Fig. 4b). Principal axis D_1 was computed as normal to the propagated wave; D_2 was calculated as the surface normal; D_3 was calculated as the cross-product of D_1 and D_2 (Table 1, Fig. 4). These vectors were computed once for the simplified mesh ("aOsteonsFile.txt"), and used during the generation of an arbitrary model (Fig. 4c). During the meshing of the current model, for each element of the cortical bone, the five nearest points of the pre-processed simplified model (defined with only 2319 nodes) were averaged. In this way, we obtained smooth and uniform osteon orientations over the complete volume. As the pre-computed osteons were projected onto the volumetric mesh of the cortical bone, the orthotropic principal vectors were not sensitive to modifications of the cortical bone geometry.

3.2 Modeling of intact teeth

Intact teeth comprise dentin, enamel and pulp tissue inside the pulp cavity (Fig. 1, Table 2). Enamel, dentin, and pulp tissue are commonly modeled as homogenous, linear, and elastic materials (recommended material characteristics from the literature are given in Table 2). The periodontal ligament (PDL) has more complex biomechanical behavior as it plays a crucial role in the load transfer from the teeth to the alveolar bone (bone adjacent to teeth) [22]. Although pioneering studies have modeled the PDL as a linear elastic material, recent studies have suggested modeling the PDL with more complex elastoplastic, hyperelastic, and viscoelastic models. As there is no consensus on which material model is the most suitable, we provided coefficients for the three most frequently used material modes in Table 2 [23–25]. We emphasize that the nonlinear finite strain viscoelastic model has recently been reported as the most suitable for modeling both the creeping behavior and nonlinear load-displacement behavior of teeth [24].

By default, OpenMandible neglects the root cementum because it has minimal thickness and its material properties are similar to the root dentin. However, by default, OpenMandible enables users

to quickly obtain nodes and elements of the mandible on the interface with the PDL. One can then select them and apply material characteristics that correspond to the cementum. Although natural materials are assumed to be bonded, by default, OpenMandible writes in the output file contacts between each material, leaving users to decide which is further used and how. OpenMandible delivers all materials and their interfaces (contacts) in separate files. By default, there are 60 input files for 14 intact teeth and 174 detected interfaces (which are bonded contacts). Thus, users can modify a specific tooth (input STL files) to create a new model for restoration, inlay, onlay, and tooth crown applications.

Table 2. Material properties of dental materials used in recent literature [23, 26-32].

E: Young's modulus [MPa]; ν: Poisson's ratio []; ρ: Density [kg m^{-3}]; q: Thermal conductivity [J m^{-1} s^{-1} $°C^{-1}$]; *c*: Specific heat [J kg^{-1} $°C^{-1}$]; α: Thermal expansion [$(m/m)^{-1}$ $°C^{-1}$]; μi and αi [ ]: Ogden hyperelastic material parameters; *Gi*: Reduced relaxation function [MPa]; τi: Decay constant [ ]; σ_c: compressive strength [MPa]; σ_t: Tensile strength [MPa]; σ_e: Endurance strength [MPa]; σ_u: Ultimate stress [MPa]; K_{th}: Fatigue threshold [MPa]; K_c: Fracture toughness [MPa]; C: Fatigue crack growth coefficient; m: Fatigue crack growth exponent.

Material	Material model	Coefficients			
		Stress analysis	Fracture analysis	Fatigue failure analysis	Fracture failure analysis
Pulp	Elastic	E = 6.8, ν = 0.45, ρ = 1000, q = 0.67, *c* = 4200, α = 1.01e-5	/	/	/
Dentin	Elastic	E = 18.6e+3, ν = 0.31, ρ = 1960, q = 0.59, *c* = 1600, α = 1.01e-5	/	σ_e = 50 σ_u = 160	$K_{th}=1.06\sqrt{m}$ $K_c=1.8\sqrt{m}$ C=6.24 m=8.76
Enamel	Elastic	E = 84.1e+3, ν = 0.30, ρ = 2800, q = 0.93, *c* = 712, α = 1.15e-5	/	/	/
PDL	Elastic	E = 0.68, ν = 0.45, ρ = 1100, q = /, *c* = /, α = /,	/	/	/
PDL	Hyperelastic	μ_1 = 0.99, μ_2 = -0.95, α_1 = 1.64 α_2 = -5, ρ = 1100	/	/	/
PDL	Viscoelastic	G_1 = 0.0897, G_2 = 0.1093, G_3 = 0.7852, τ_1 = 0.1548, τ_2 = 0.0038, $\tau_3 = 3.521 \times 10^{-5}$, ρ = 1100	/	/	/

Composite resin	Elastic	E = 16.6e+3, ν = 0.24, ρ = 2100, q = 1.087, *c* = 200, α = 2.70e-5	/	/	/
Gutta-percha	Elastic	E = 70.0, ν = 0.40, ρ = 2700, q = 332.4, *c* = 1042, α = 16.20e-5	/	/	/
Cortical bone	Orthotropic	See Table 1	σ_{c1} = 133 σ_{c2} = 133 σ_{c3} = 199.5 σ_{t1} = 92 σ_{t2} = 92 σ_{t3} = 138	σ_e = 106 σ_u = 140	/
Cortical bone	Elastic	E = 13.7e+3, ν = 0.30, ρ = 1900	/	/	/
Cancellous bone	Elastic	E = 1.37e+3, ν = 0.30, ρ = 1100	/	/	/
TMJ articular cartilage	Elastic	E = 6.00, ν = 0.30	/	/	/

3.3 Modeling constraints

OpenMandible enables modeling of 1) the overall masticatory system (Fig. 5a), or 2) isolated parts of the mandible (Fig. 5b). As shown in Fig. 5a, modeling of the complete mandible should include setting constraints at three points: at the bite point and the two joints [33]. Such a scenario most realistically reproduces the masticatory system during food processing. During chewing, food is moved through the mouth by the cheeks and tongue. During one bite, pressure is applied to only one small region at a time. The chewing process is repeated many times on different spots (teeth). Thus, when modeling a single bite, it is appropriate to constrain a small area on the occlusal surface of the teeth.

The second important question is how to properly constrain the mandible joints. The temporomandibular joint (TMJ) is composed of three main structures: the mandibular condyle (convex segment of the mandible), the concave articular surface of the temporal bone, and the articular cartilage disc between them (which has a buffering effect and prevents high occlusal stress to the cranium). Alternatively, the condyles can be directly constrained in all three directions, but this neglects the buffering effect of the articular cartilage, resulting in stress concentration in the condyles. The OpenMandible framework solves this problem with a simplified TMJ (users can add/modify the input STL files and create more complex TMJ geometry). Generally, each TMJ is made of a block of the

temporal bone and a disc representing the TMJ articular disc and cartilage (Fig. 5a). Each block of the temporal bone is constrained in all three directions.

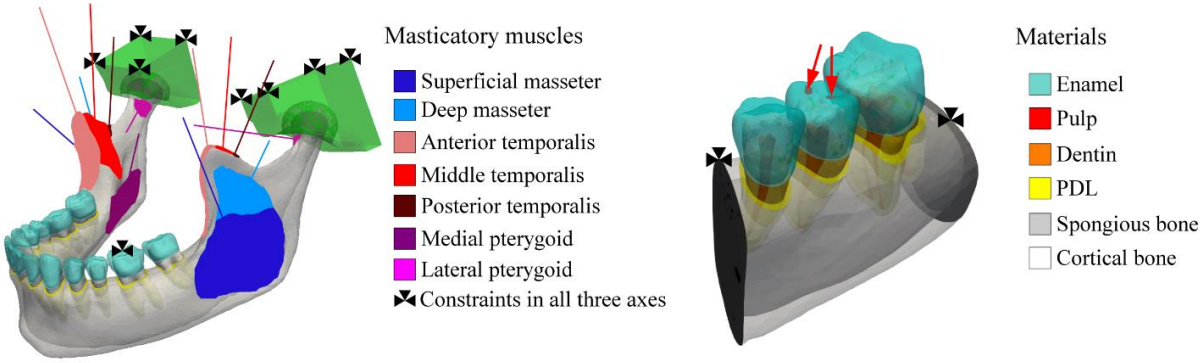

Fig. 5 – Sketch of BCs needed to model the complete masticatory system and its cut-part.

To study the behavior of a particular tooth, we recommend cutting two surrounding teeth and corresponding parts of the cortical and cancellous bone, as shown in Fig. 5b. Although many studies preferred to model only a single tooth placed in an artificial carrying material [26], incorporation of realistic bone support is highly recommended to achieve accurate results. Regarding constraints to be applied, one must select cut planes and restrict displacements on all nodes (Fig. 5b). In addition, a single-tooth analysis requires modeling of tooth-to-tooth contact instead of fixation, as for the occlusal surface [34]. Although many studies have compensated for this process by applying forces to the occlusal surface, recent studies have reported that contact analysis more accurately reproduces physiological conditions during chewing [34].

3.4 Assessment of structural integrity during mastication: fatigue and fracture analysis

Assessment of structural integrity involves the calculation of risk and prediction of when the structure will fail under prescribed loads. In nature, structures usually fail by 1) fatigue failure [35], 2) fracture failure [35, 36], and 3) fatigue to fracture. Compared to conventional stress analysis, the post-processing step quantitatively assesses risk by accounting the FEA results and material properties derived from physical fatigue and/or fracture tests. The failure of a multi-material structure, such as a mandible, can be defined as the moment when a carrying part/material fails. With a mandible, the carrying material is the cortical bone. The failure of a tooth may be related to the inability of dentin, enamel, or artificial material used to replace dentin and enamel. As it is an important topic in the field of dentistry, but not a direct subject of this study, Appendix C provides a detailed review and recommendations on how the structural integrity of dental materials should be assessed.

3.4.1 Fatigue and fracture loads

The mandible-breaking force ranges from 2–2.5 kN and depends on the specific problem [19]. Given values correspond to the punch force, (we recommend finding fracture forces for a particular problem in the literature), which should be applied perpendicularly to the frontal and lateral side on a circular area (~1 cm in diameter). For the fracture analysis of a tooth, it is recommended to experimentally determine the critical breaking force for the considered tooth, which should be applied to the model. In the literature, the range of a tooth-breaking force is 700–1200 N [26], and varies for intact and treated teeth. Mastication forces are reported to be 100–250 N [4]. However, the manner in which these loads are prescribed may vary:

- The simplest method is to apply force on a single node or element, or on a small area of the occlusal surface of the tooth. Within OpenMandible, this can be done as described in Section 2.4.
- The force can be applied through a sphere (representing the cusp of the opposing tooth) that transfers pressure to the occlusal surface and contacts the tooth at two, three, or four points. This method uses nonlinear contact analysis, which was reported as a means of obtaining a more realistic stress distribution [16, 34].
- The most realistic means of simulating mastication BCs is by incorporating muscle forces (Fig. 5a) [33, 38].

3.5 Modeling of masticatory muscles

OpenMandible considers all four main groups of masticatory muscles (responsible for the elevation of the mandible): masseter, temporalis, medial pterygoid, and lateral pterygoid (Fig. 6, Table 3). In the literature, muscles are commonly modeled as directed forces [33], springs [8, 19], and solid elements [39]. In all three cases, the key is to realistically define the muscle orientation and the biomechanical behavior response. We provide a skull model for defining the muscles in Fig. 6. The muscle BCs are generated by taking a group of nodes from the mandible as input and uniformly connecting them to corresponding nodes/areas on the skull (STL files in the folder input/bc_directed). In the output files (folder output/bc_directed), we deliver pairs of these nodes, with the unit direction vectors, to be imported into simulation software as directed springs or forces (solid models of muscles can also be created using the input surface patches).

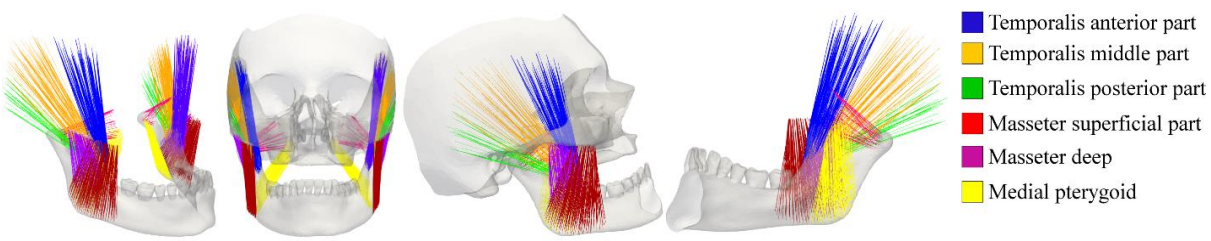

Fig. 6 – Masticatory muscles considered in the OpenMandible framework.

Table 3. Recommended values of muscle forces.

	Apicella et al. 2010 [41]	Commisso et al. 2015 [42]	Rues et al. 2010 [40]				
Masseter	10 N		121 N	75 N	90 N	85 N	83 N
Masseter superficial part		190.4 N					
		81.6 N					
Medial pterygoid	6 N	174.8 N	30 N	24 N	23 N	28 N	28 N
Lateral pterygoid	/		10 N	5 N	5 N	5 N	6 N
Lateral pterygoid, superior part		66.9 N					
Lateral pterygoid, inferior part		28.8 N					
Temporalis, anterior part	8 N	158.0	120 N	120 N	95 N	105 N	83 N
Temporalis, middle part	/	95.6	/	/	/	/	/
Temporalis, posterior part	8 N	75.6	30 N	30 N	25 N	40 N	27 N
Comment		Unilateral molar biting	Bilateral canine biting, with a resulting force 200 N	Bilateral premolar biting, with a resulting force 200 N	Bilateral molar biting, with a resulting force 200 N	Unilateral molar biting, ipsilateral side; with a resulting force 200 N	Unilateral molar biting, contralateral side; with a resulting force 200 N

3.6 Modeling of teeth restoration

Teeth restoration assumes the removal of teeth tissue affected by caries and replacement with artificial materials. The cavity preparation is commonly filled with composite resin; root canals are filled with cold gutta-percha. Developing the restored teeth within the proposed framework can be achieved by modifying the geometries of the provided intact teeth. One must alter the intact teeth mesh to specify a composite material and incorporate generated meshes into the input folders.

Regarding the biomechanics of restored teeth, it is emphasized that during and after resin-composite material curing, the shrinkage of the material causes residual stress known as shrinkage stress [43, 44]. From a practical standpoint, shrinkage stresses are significant, as they can cause microcracks

in the surrounding enamel [45]. As it has been experimentally shown that shrinkage stress cannot be neglected [43], it must be accounted for before performing simulations with post-restorative models.

In the literature, the volumetric change of the restoration (caused by polymerization shrinkage) was simulated as an analogy of thermal expansion in heat transfer analysis [46]. In OpenMandible, this assumes selection of the outer-irradiated surface of the composite resin, subsequently setting the thermal expansion to 0.005, and reducing the temperature one degree on the irradiated surface in the simulation package (material characteristics are given in Table 1). The shrinkage stress values may vary and can only be accurately assessed through experiments [47]. Accordingly, it is recommended to run a series of simulations with varying shrinkage stress levels to investigate how they influence the studied problem [29].

3.7 Modeling of implants

The majority of dentistry related studies have focused on the modeling of dental implants [48, 49]. To date, most of these studies have modeled the interface between the implant surface and bone as a bonded structure, which simulates osseointegration [34]. A metal implant (commonly titanium), as a much stiffer part, absorbs most of the stress and prevents bone deformation. In contrast, clinical practice shows that the majority of implant failures are related to bone degradation [50, 51]. An alternative approach uses contact analysis [34], which has been used in two scenarios for modeling the bone–implant interface. The first scenario is a complete bond with an infinite tension strength and shear at the osseointegration interface or in bioactive material; the second is a free contact simulation of relative displacement without tensile force resistance to describe healing or an immediately loaded condition. Both contact approaches require knowing the IDs of nodes and faces on the interfaces between the implant and bone material. By default, the OpenMandible framework delivers all bonded contacts between input materials and writes them into the output folder “Contacts” for further use.

4. Results and discussion

The complete source code, executables, and data presented in this study are available on the public repository: https://github.com/ArsoVukicevic/OpenMandible. Compared to previous initiatives that shared only raw medical scans [7–10], or a particular teeth model [11], there are several advantages that make OpenMandible more suited to the dentistry community.

To the best of our knowledge, this is the first study to make publicly available a detailed intact model of the complete human lower mandible physiology. This is important for several reasons. First, an accurate and publicly available data set can serve as the starting point for further studies on computational medicine in dentistry, accelerating the development of simulation models and enabling the objective comparison of findings reported by independent studies. As most of dentistry studies have

focused on investigating the response of restorative materials and implants, their conclusions should always be compared with the referent (intact) model to objectively assess how a particular treatment changed the biomechanical behavior of the whole mandible. From this perspective, modification of the baseline model to study dentistry treatments (as illustrated in Fig. 7) may be more suitable. It is also more efficient than the traditional development of simulation models from medical scans.

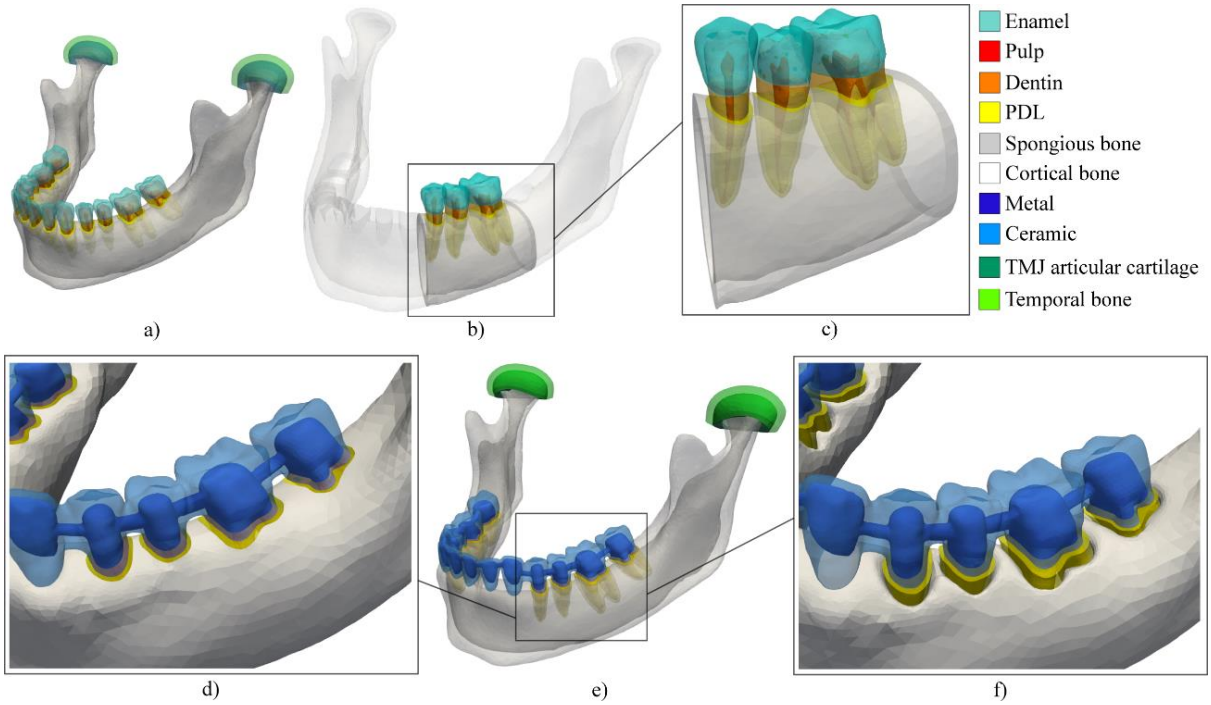

Fig. 7 – Generation of new models from the baseline model: a) Base intact model; b) Modified mandible; c) Three teeth of interest for modeling the restoration of L5; d) Mandible with implanted metal-ceramic fixed dental prosthesis; e) Mandible with metal-ceramic fixed dental prosthesis and bone loss caused by periodontitis

The use cases of OpenMandible are shown in Fig. 7. The development of new models from the baseline model in Fig. 7a assumes a slight modification of the corresponding inputs (STL files that contain geometry and BCs). For example, if one is interested in modeling (for restoration) a single tooth (lower left second premolar), one could cut only the relevant tooth and the two surrounding teeth (lower left first premolar and first molar) and the accompanying cortical/trabecular bone (Fig. 7b, 7c; BCs are shown in Fig. 5b). This is demonstrated in Fig. 7d-e, which shows the model of the mandible without incisors and canines. The rehabilitation was performed with a metal–ceramic fixed dental prosthesis. Fig. 7f shows how Fig. 7e can be further modified for studying bone loss due to periodontitis. To illustrate the benefits for future users, we emphasize that the development of showcase models took us 1–3 working days; the development of the baseline model (Fig. 7a) required several months.

Contribution that separates OpenMandible from previous studies [7–11], which provided only public data sets, is the accompanying C++ open-source framework that simplifies the generation of BCs. OpenMandible was developed on top of a highly efficient dfemtoolz library, the computational

complexity and efficiency of which was analyzed in our previous study [12]. The source code was developed to be compatible with both Linux and Windows operating systems to allow usage by a wider audience. To increase the impact and usability, we demonstrated that the models generated by OpenMandible are easily imported into the most popular commercial packages such as ANSYS for further analysis.

In addition to standard features for prescribing materials and boundary conditions on selected regions, OpenMandible provides a series of features that are not present or difficult to reproduce in conventional packages. The first feature is the automatic application of orthotropic material characteristics on the cortical bone, for which we proposed a novel geodesic wave propagation algorithm (Fig. 4). In this way, we enabled the incorporation of micromechanical material properties that are impossible to import from conventional medical scans. Compared to previous studies that determined orthotropy axes by modeling the harmonic fields through mandibles [21], our approach is more simplistic and does not depend on additional simulation software. More important, it is robust to variations in model geometry. For example, if one attempts to model the harmonics field over Fig. 7a and Fig. 7c, the resulting orientations of osteons will differ because the domain and the BCs of the harmonic fields are affected by the change in geometry. OpenMandible can deliver the same material properties (orientation of osteons) for both models because the framework uses pre-computed wave propagation over the simplified intact mandible to determine coarse osteons, which are transferred to the detailed model.

In addition to the orientation of osteons, we also incorporated algorithms that split the jaw into 16 anatomical zones, which is essential because the material characteristics vary across the mandible. Using conventional approaches presented in the literature [18], this level of detail can only be achieved by physically splitting the mandible into 16 parts, which is time consuming and drastically increases the number of nodes and elements in the resulting model.

Another important feature proposed in this study is the modeling of muscle fibers as vectors oriented from an area selected on the mandible to a chosen area on the skull mesh. In this way, muscles are modeled more realistically, as uniformly distributed lines (Fig. 5), instead of lines concentrated to one end-point, which is the default feature available in commercial packages and was used in previous studies [8, 18, 33, 37–39] (Fig. 4a). By default, for each node that corresponds to the muscle insertion, OpenMandible delivers a unit vector that can be further multiplied and imported into simulation software.

Another valuable contribution of this study is the in-depth review of BCs and modeling approaches used in the most relevant studies on the topic, with an emphasis on how they can be reproduced using

the proposed framework, which will help to homogenize future studies and enable more objective comparison of their results.

Although we recommend usage/modification of the provided base OpenMandible model, potential users can use the framework with their own geometries/models and/or integrate the provided source code into their own projects. Accordingly, we also encourage the community to contribute by incorporating their own features or simulation models into the public repository. Future improvements in OpenMandible will be directed toward better integration with other widely used commercial and public simulation packages, and toward the development of a graphical interface to enhance usage and manipulation with the model inputs and outputs.

5. Conclusions and future work

In this study, we proposed a novel OpenMandible framework, which enables the development of realistic simulation models of lower mandible physiology through slight editing of the base intact model and setting the corresponding inputs. The complete source code, executables, showcases, and sample data are freely available on the public repository so that others can contribute to the further development of features and base models. The outputs of the OpenMandible framework can be imported into any simulation software package (for ANSYS, we currently provide a dedicated demonstration/tutorial that shows how the generated models, mechanical properties, and BCs can be imported for further FEA). The proposed base model and user-friendly C++ framework can serve as a basis for a wide range of new studies on topics related to human lower mandible physiology. In adopting OpenMandible, simplifications and inconsistency in terms of geometry, materials, and boundary conditions are significantly reduced and reproducibility is increased.

Acknowledgements

This study was funded by grants from Ministry of Education and Science of the Republic of Serbia
45005, III41007 and ON174028.

6. References

1. Viceconti M, Hunter P. The Virtual Physiological Human: Ten Years After. Annu Rev Biomed Eng. 2016 Jul 11;18:103-23. doi: 10.1146/annurev-bioeng-110915-114742.
2. Ausiello P, Gloria A, Maietta S, Watts DC, Martorelli M. Stress Distributions for Hybrid Composite Endodontic Post Designs with and without a Ferrule: FEA Study. Polymers (Basel). 2020 Aug 16;12(8):1836. doi: 10.3390/polym12081836.
3. Adamovich A, Park S, Siskin GP, Englander MJ, Mandato KD, Herr A, Keating LJ. The ABCs of the

FDA: A Primer on the Role of the United States Food and Drug Administration in Medical Device Approvals and IR Research. J Vasc Interv Radiol. 2015 Sep;26(9):1324-30. doi: 10.1016/j.jvir.2015.05.028.

4. van der Bilt A, Engelen L, Pereira LJ, van der Glas HW, Abbink JH. Oral physiology and mastication. Physiol Behav. 2006 Aug 30;89(1):22-7. doi: 10.1016/j.physbeh.2006.01.025.
5. Trivedi S. Finite element analysis: A boon to dentistry. J Oral Biol Craniofac Res. 2014 Sep-Dec;4(3):200-3. doi: 10.1016/j.jobcr.2014.11.008.
6. Opdam NJM, Collares K, Hickel R, Bayne SC, Loomans BA, Cenci MS, Lynch CD, Correa MB, Demarco F, Schwendicke F, Wilson NHF. Clinical studies in restorative dentistry: New directions and new demands. Dent Mater. 2018 Jan;34(1):1-12. doi: 10.1016/j.dental.2017.08.187.
7. The Visible Human Project. www.nlm.nih.gov/research/visible/ [accessed 22 August 2020].
8. Kober C, Erdmann B, Lang J, Sader R, Zeilhofer H–F. Adaptive Finite Element Simulation of the Human Mandible Using a New Physiological Model of the Masticatory Muscles. PAMM · Proc Appl. Math. Mech. 2004;4:332–333, doi: 10.1002/pamm.200410147.
9. Tang L, Chung MS, Liu Q, Shin DS. Advanced features of whole body sectioned images: Virtual Chinese Human. Clin Anat. 2010 Jul;23(5):523-9. doi: 10.1002/ca.20975.
10. Virtual population. https://itis.swiss/virtual-population/ [accessed 22 August 2020].
11. Boryor A, Hohmann A, Geiger M, Wolfram U, Sander C, Sander FG. A downloadable meshed human canine tooth model with PDL and bone for finite element simulations. Dent Mater. 2009 Sep;25(9):e57-62. doi: 10.1016/j.dental.2009.05.002.
12. Milasinovic DZ, Vukicevic AM, Filipovic ND. dfemtoolz: An open-source C++ framework for efficient imposition of material and boundary conditions in finite element biomedical simulations. Comput. Phys. Commun. 2020;249:106996. doi: 10.1016/j.cpc.2019.106996.
13. Zix JA, Schaller B, Lieger O, Saulacic N, Thorén H, Iizuka T. Incidence, aetiology and pattern of mandibular fractures in central Switzerland. Swiss Med Wkly. 2011 May 27;141:w13207. doi: 10.4414/smw.2011.13207.
14. van Hout WM, Van Cann EM, Abbink JH, Koole R. An epidemiological study of maxillofacial fractures requiring surgical treatment at a tertiary trauma centre between 2005 and 2010. Br J Oral Maxillofac Surg. 2013 Jul;51(5):416-20. doi: 10.1016/j.bjoms.2012.11.002.
15. Shaikh ZS, Worrall SF. Epidemiology of facial trauma in a sample of patients aged 1-18 years. Injury.

2002 Oct;33(8):669-71. doi: 10.1016/s0020-1383(01)00201-7.

16. Nomura T, Gold E, Powers MP, Shingaki S, Katz JL. Micromechanics/structure relationships in the human mandible. Dent Mater. 2003 May;19(3):167-73. doi: 10.1016/s0109-5641(02)00026-x.
17. Bonnet AS, Postaire M, Lipinski P. Biomechanical study of mandible bone supporting a four-implant retained bridge: finite element analysis of the influence of bone anisotropy and foodstuff position. Med Eng Phys. 2009 Sep;31(7):806-15. doi: 10.1016/j.medengphy.2009.03.004.
18. Schwartz-Dabney CL, Dechow PC. Variations in cortical material properties throughout the human dentate mandible. Am J Phys Anthropol. 2003 Mar;120(3):252-77. doi: 10.1002/ajpa.10121. PMID: 12567378.
19. Antic S, Vukicevic AM, Milasinovic M, Saveljic I, Jovicic G, Filipovic N, Rakocevic Z, Djuric M. Impact of the lower third molar presence and position on the fragility of mandibular angle and condyle: A Three-dimensional finite element study. J Craniomaxillofac Surg. 2015 Jul;43(6):870-8. doi: 10.1016/j.jcms.2015.03.025.
20. Ding X, Liao S-H, Zhu X-H, Wang H-M, Zou B-J. Effect of orthotropic material on finite element modeling of completely dentate mandible. Mater. Des. 2015;84:144-153. doi: 10.1016/j.matdes.2015.06.091.
21. Liao SH, Zou BJ, Geng JP, Wang JX, Ding X. Physical modeling with orthotropic material based on harmonic fields. Comput Methods Programs Biomed. 2012 Nov;108(2):536-47. doi: 10.1016/j.cmpb.2011.04.005.
22. Kober C, Erdmann B, Hellmich C, Stuebinger S, Sader R, Zeilhofer H-F. Dental versus mandibular biomechanics: the influence of the PDL on the overall structural behaviour. J. Biomech. 2006;39:S455. doi: 10.1016/S0021-9290(06)84864-5.
23. Karimi A, Razaghi R, Biglari H, Mohammadali Rahmati S, Sandbothe A, Hasani M. Finite element modeling of the periodontal ligament under a realistic kinetic loading of the jaw sys-tem. Saudi Dent J. 2019; in-press. doi: 10.1016/j.sdentj.2019.10.005.
24. Su M-Z, Chang H-H, Chiang Y-C, Cheng J-H, Fuh L-J, Wang C-Y, Lin C-P. Modeling viscoelastic behavior of periodontal ligament with nonlinear finite element analysis. J. Dent. Sci. 2013;8(2):121-128. doi: 10.1016/j.jds.2013.01.001.

25. Natali AN, Pavan PG, Venturato C, Komatsu K. Constitutive modeling of the non-linear visco-elasticity of the periodontal ligament. Comput Methods Programs Biomed. 2011 Nov;104(2):193-8. doi: 10.1016/j.cmpb.2011.03.014.
26. Zelic K, Vukicevic A, Jovicic G, Aleksandrovic S, Filipovic N, Djuric M. Mechanical weakening of devitalized teeth: three-dimensional Finite Element Analysis and prediction of tooth fracture. Int Endod J. 2015 Sep;48(9):850-63. doi: 10.1111/iej.12381.
27. Arola D, Zheng W, Sundaram N, Rouland JA. Stress ratio contributes to fatigue crack growth in dentin. J Biomed Mater Res A. 2005 May 1;73(2):201-12. doi: 10.1002/jbm.a.30269.
28. Arola D, Huang MP. The influence of simultaneous mechanical and thermal loads on the stress distribution in molars with amalgam restorations. J Mater Sci Mater Med. 2000 Mar;11(3):133-40. doi: 10.1023/a:1008905423584.
29. Vukicevic AM, Zelic K, Jovicic G, Djuric M, Filipovic N. Influence of dental restorations and mastication loadings on dentine fatigue behaviour: Image-based modelling approach. J Dent. 2015 May;43(5):556-67. doi: 10.1016/j.jdent.2015.02.011.
30. Toms SR, Eberhardt AW. A nonlinear finite element analysis of the periodontal ligament under orthodontic tooth loading. Am J Orthod Dentofacial Orthop. 2003 Jun;123(6):657-65. doi: 10.1016/s0889-5406(03)00164-1.
31. Huang H, Tang W, Tan Q, Yan B. Development and parameter identification of a visco-hyperelastic model for the periodontal ligament. J Mech Behav Biomed Mater. 2017 Apr;68:210-215. doi: 10.1016/j.jmbbm.2017.01.035.
32. Zioupos P, Cook RB, Hutchinson JR. Some basic relationships between density values in cancellous and cortical bone. J Biomech. 2008;41(9):1961-8. doi: 10.1016/j.jbiomech.2008.03.025.
33. Gröning F, Fagan M, O'Higgins P. Modeling the human mandible under masticatory loads: which input variables are important? Anat Rec (Hoboken). 2012 May;295(5):853-63. doi: 10.1002/ar.22455.
34. Murakami N, Wakabayashi N. Finite element contact analysis as a critical technique in dental biomechanics: a review. J Prosthodont Res. 2014 Apr;58(2):92-101. doi: 10.1016/j.jpor.2014.03.001.
35. Teoh SH. Fatigue of biomaterials: a review. Int. J. Fatigue 2000; 22(10):825-837. doi: 10.1016/S0142-1123(00)00052-9.
36. Xu B, Wang Y, Li Q. Modeling of damage driven fracture failure of fiber post-restored teeth. J Mech Behav Biomed Mater. 2015 Sep;49:277-89. doi: 10.1016/j.jmbbm.2015.05.006.

37. Li H, Li J, Zou Z, Fok AS. Fracture simulation of restored teeth using a continuum damage mechanics failure model. Dent Mater. 2011 Jul;27(7):e125-33. doi: 10.1016/j.dental.2011.03.006.
38. Gröning F, Jones ME, Curtis N, Herrel A, O'Higgins P, Evans SE, Fagan MJ. The importance of accurate muscle modelling for biomechanical analyses: a case study with a lizard skull. J R Soc Interface. 2013 Apr 24;10(84):20130216. doi: 10.1098/rsif.2013.0216.
39. Röhrle O, Pullan AJ. Three-dimensional finite element modelling of muscle forces during mastication. J Biomech. 2007;40(15):3363-72. doi: 10.1016/j.jbiomech.2007.05.011.
40. Rues S, Lenz J, Türp JC, Schweizerhof K, Schindler HJ. Muscle and joint forces under variable equilibrium states of the mandible. Clin Oral Investig. 2011 Oct;15(5):737-47. doi: 10.1007/s00784-010-0436-4.
41. Apicella D, Aversa R, Ferro F, Ianniello D, Perillo L, Apicella A. The importance of cortical bone orthotropicity, maximum stiffness direction and thickness on the reliability of mandible numerical models. J Biomed Mater Res B Appl Biomater. 2010 Apr;93(1):150-63. doi: 10.1002/jbm.b.31569. Erratum in: J Biomed Mater Res B Appl Biomater. 2011 Jul;98(1):201. Perillo, Letizia.
42. Commisso MS, Martínez-Reina J, Ojeda J, Mayo J. Finite element analysis of the human mastication cycle. J Mech Behav Biomed Mater. 2015 Jan;41:23-35. doi: 10.1016/j.jmbbm.2014.09.022.
43. Al Sunbul H, Silikas N, Watts DC. Polymerization shrinkage kinetics and shrinkage-stress in dental resin-composites. Dent Mater. 2016 Aug;32(8):998-1006. doi: 10.1016/j.dental.2016.05.006.
44. Meereis CTW, Münchow EA, de Oliveira da Rosa WL, da Silva AF, Piva E. Polymerization shrinkage stress of resin-based dental materials: A systematic review and meta-analyses of composition strategies. J Mech Behav Biomed Mater. 2018 Jun;82:268-281. doi: 10.1016/j.jmbbm.2018.03.019.
45. Chuang SF, Chang CH, Yaman P, Chang LT. Influence of enamel wetness on resin composite restorations using various dentine bonding agents: part I-effects on marginal quality and enamel microcrack formation. J Dent. 2006 May;34(5):343-51. doi: 10.1016/j.jdent.2005.07.006.
46. Chuang SF, Chang CH, Chen TY. Contraction behaviors of dental composite restorations--finite element investigation with DIC validation. J Mech Behav Biomed Mater. 2011 Nov;4(8):2138-49. doi: 10.1016/j.jmbbm.2011.07.014.
47. Yang J, Silikas N, Watts DC. Pre-heating time and exposure duration: Effects on post-irradiation properties of a thermo-viscous resin-composite. Dent Mater. 2020 Jun;36(6):787-793. doi: 10.1016/j.dental.2020.03.025.

48. Williams DF. Implants in dental and maxillofacial surgery. Biomaterials. 1981 Jul;2(3):133-46. doi: 10.1016/0142-9612(81)90039-9.
49. Mendonça G, Mendonça DB, Aragão FJ, Cooper LF. Advancing dental implant surface technology--from micron- to nanotopography. Biomaterials. 2008 Oct;29(28):3822-35. doi: 10.1016/j.biomaterials.2008.05.012.
50. Revathi A, Borrás AD, Muñoz AI, Richard C, Manivasagam G. Degradation mechanisms and future challenges of titanium and its alloys for dental implant applications in oral environment. Mater Sci Eng C Mater Biol Appl. 2017 Jul 1;76:1354-1368. doi: 10.1016/j.msec.2017.02.159.
51. Heinemann F, Hasan I, Bourauel C, Biffar R, Mundt T. Bone stability around dental implants: Treatment related factors. Ann Anat. 2015 May;199:3-8. doi: 10.1016/j.aanat.2015.02.004.
52. Hang S. TetGen, a Delaunay-Based Quality Tetrahedral Mesh Generator. ACM Trans Math Softw. 2015;4. doi: 10.1145/2629697.
53. Tang Z, Tu W, Zhang G, Chen Y, Lei T, Tan Y. Dynamic simulation and preliminary finite element analysis of gunshot wounds to the human mandible. Injury. 2012 May;43(5):660-5. doi: 10.1016/j.injury.2011.03.012.
54. Pajic SS, Antic S, Vukicevic AM, Djordjevic N, Jovicic G, Savic Z, Saveljic I, Janović A, Pesic Z, Djuric M, Filipovic N. Trauma of the Frontal Region Is Influenced by the Volume of Frontal Sinuses. A Finite Element Study. Front Physiol. 2017 Jul 11;8:493. doi: 10.3389/fphys.2017.00493.
55. Gross D, Seelig T. Classical fracture and failure hypothesis. In: Ling FF (ed.), Fracture mechanics With an introduction to micromechanics, 2nd, editor. Berlin, Heidelberg: Springer Verlag, 2011, 39e49.
56. Goodman J. Mechanics applied to engineering. London: Longman Greens; 1899.
57. Nalla RK, Kinney JH, Marshall SJ, Ritchie RO. On the in vitro fatigue behavior of human dentin: effect of mean stress. J Dent Res. 2004 Mar;83(3):211-5. doi: 10.1177/154405910408300305.
58. Nalla RK, Imbeni V, Kinney JH, Staninec M, Marshall SJ, Ritchie RO. In vitro fatigue behavior of human dentin with implications for life prediction. J Biomed Mater Res A. 2003 Jul 1;66(1):10-20. doi: 10.1002/jbm.a.10553.
59. Zioupos P, Gresle M, Winwood K. Fatigue strength of human cortical bone: age, physical, and material heterogeneity effects. J Biomed Mater Res A. 2008 Sep;86(3):627-36. doi: 10.1002/jbm.a.31576.

60. Carter DR, Caler WE, Spengler DM, Frankel VH. Fatigue behavior of adult cortical bone: the influence of mean strain and strain range. Acta Orthop Scand. 1981 Oct;52(5):481-90. doi: 10.3109/17453678108992136.
61. Kojic M, Bathe KJ. Inelastic analysis of solids and structures. Springer; 2005.
62. Paris PC, Erdogan F. A critical analysis of crack propagation laws. J. Fluids Eng. 1963;85:528–33, doi:10.1115/1.3656900,
63. Vukicevic AM, Jovicic GR, Jovicic MN, Milicevic VL, Filipovic ND. Assessment of cortical bone fracture resistance curves by fusing artificial neural networks and linear regression. Comput Methods Biomech Biomed Engin. 2018 Feb;21(2):169-176. doi: 10.1080/10255842.2018.1431220.
64. Li B, de Freitas M. A Procedure for Fast Evaluation of High-Cycle Fatigue Under Multiaxial Random Loading. J. Mech. Des. 2002;124:558-563. doi: 10.1115/1.1485291.

Appendix 1. How to develop a model starting from the OpenMandible baseline model

This appendix supports Fig. 7a-c, and is a minimalistic use case to illustrate the OpenMandible workflow (Fig. 2). The intention was to analyze a single tooth (lower left second premolar) during its restoration. The first step is to adapt (cut) the reference mandible model in Fig. A1a. The remaining holes of the cortical and cancellous bone were patched, as shown in Fig. A1b. After the surface meshes were ready, the element type (tet4 or hex8) was selected in Section A of the config file. Newly generated meshes with the three teeth of interest were stored in the input folder "../input/materials/stl", and their names and types listed in Section B of the../input/open_mandible_program_parameters.cfg file (config file). Subsequently, the input surface meshes were discretized into volumetric; in this study, we used the TetGen mesh generator [52], with outputs (*.node and *.ele files) placed in "../input/materials/tetgen-files and used to assemble the model. Because the surface nodes of the neighboring materials must be the same, a volumetric mesh must be generated without adding new nodes to the material surfaces (with TetGen, -Y flag should be used as a parameter). For the 14-input surface meshes, OpenMandible generated 19 materials by splitting the cut-part of the cortical bone into six anatomical zones (Fig. 4 and Fig. A1c). Boundary conditions were stored in the folder "../input/bc", and commands for their application on the generated volumetric model were written into Section C of the config file:

```
Section_C_list_start
-
CorticalBone BC_Cortical_CancellousBone_FixedSupport.stl 1.0
CancellousBone BC_Cortical_CancellousBone_FixedSupport.stl 1.0
```

```
Tooth_L5_Enamel BC_Tooth_L5_Enamel_Forces.stl -1.0
-
Section_C_list_end
```

As illustrated in Fig. A1d, these commands constrain the movement of cortical and spongy bone compartments on the cut planes (black color), and apply forces on the left second premolar (red arrows). As this use case does not require modeling of muscle support, Section D of the config file remained empty. The orthotropic material characteristics for the cortical were prescribed in Section E using the following command:

```
Section_E_choice_run_module 1
Section_E_pick_material_name CorticalBone
```

Depending on user preference, output formats can be selected in Section F (*.txt, *.pos, and *.vtk are supported).

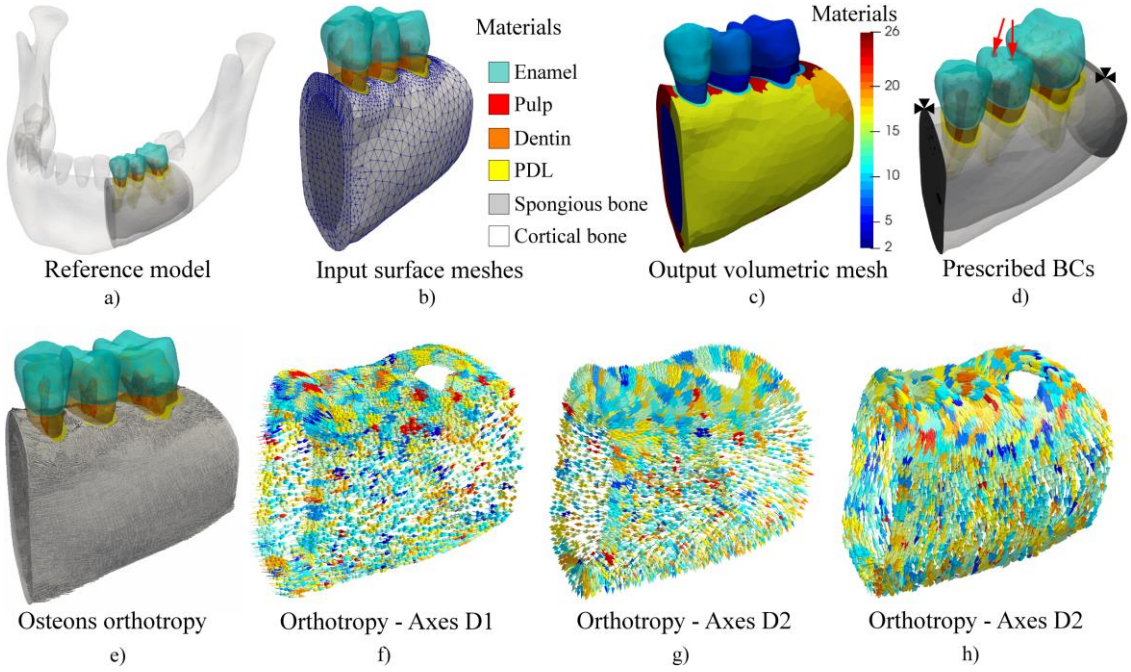

Fig. A1 – Development of a simplified model for studying a particular region of interest.

The OpenMandible executable should be placed in the root folder and executed after setting up the config file and input files. The resulting 3-D orientations of the osteons shown in Fig. A1e-h indicate the high quality and uniformity of the generated orthotopic axes, confirming the robustness to the modification of the cortical mesh. If we selected the tet4 element type, the output folder would contain a list of all 1) nodes, 2) elements (with materials ID), 3) constrained nodes, and 4) surfaces where loads must be applied. These lists must be imported into simulation software, in our case ANSYS, for which we developed a dedicated STL exporter and a how-to guide (available on the repository).

Appendix 2 OpenMandible source code and its usage

Both standalone and source code of the OpenMandible are provided, with two use-cases showing how to generate the whole masticatory system and its cut-part (Fig. 5). The software was developed by using the Linux g++ compiler and the Code::Blocks IDE. Since no third-party libraries were used, the framework could be compiled for any platform (C++ makefiles are provided for both Windows and Linux OS). The C++ project includes the dfemtoolz library and its three modules (remesh, openR, multi-material) - which are described in our previous study [12]. Generation of new simulation models starts with the definition of dynamic template arrays (Collection-s and SuperCollection-s classes from the dfemtoolz library), which stores all the model data and features:

```
SuperCollection <Mesh_Node> nodez;
SuperCollection <Geom_Element> elements;
Collection <Geom_Element> contact_faces, surface_faces;
```

Workflow, and key data structures, of the framework will be explained following the analogy of the config file sections (which are described in Section 2.4):

Step 1: TetGen (or other meshing software) outputs are used to create tet4 or tet8 mesh of the model. Briefly, the dfemtoolz_remesh module process each material provided as the Section A inputs:

```
dremesh_get_elemsF(
params->submodule,// this is user selection for tet4 or hex8 from .cfg file
nodez[i], // Nodes of i-th material
elements[i], // Elements of i-th material
"input/materials/tetgen-files/" + params->materials_names[i] + ".1.node",
"input/materials/tetgen-files/" + params->materials_names[i] + ".1.ele",
 "");
```

Step 2: Meshes of the constitutive materials are merged into the single multi-material model by using the dfemtoolz_multimaterial module:

```
merg_multimaterial(
params, // singleton object that contains all the programme parameters
nodez,           //           supercollection           of           nodes
Elements,          //          supercollection          of          elements
surface_faces,       //       collection       of       surface       faces
contact_faces,       //       collection       of       contact       faces
all_contacts); // supercollection of all contact faces
```

Step 3: Application of BCs from the input .stl files (from input/bc) was done by calling the dfemtoolz_openR module for each input command written into the C section of the config file:

```
bc_openR(
params, // singleton object that contains all the programme parameters
nodez[1], // first collection of nodes in supercollection
elements[1], // first collection of elements in supercollection
surface_faces, // collection of surface faces
contact_faces); // collection of contact faces
```

Step 4: Application of the directed BCs, which is similar to the step 3, with the difference that it uses two .stl files as inputs (the first .stl defines the insertion nodes, and the latter determines the origin of the directed BCs - in our case muscles).

```
bc_directed(params, nodez[1], elements[1]);
```

Step 5 - Software reads the osteons (input/aOsteonsFile.txt) pre-computed for the simplified mandible model, and uses its data to 1) split the selected material (by default CorticalBone) into anatomical zones, and 2) prescribe orthotropy axes for each element of the selected material:

```
material_ID_max = orthotropy(params, nodez[1], elements[1]);
```

All outputs are printed using the objects of singleton classes POS_Printer, VTK_Printer, and a set of functions used for plain text printing (listed in "case5-mandible_plain_text_print_functions.h"). Each function name is self-descriptive, so for example:

```
if (elements[1][1].how_many_nodes_per_element() == constants::TETRA)
 print_plain_text_BC_nodes_file(
 params->prescribed_surfaces_filenames[i].name,
 params->prescribed_surfaces_filenames[i].material,
 normal_vector,
 BCnodes,
 "output/bc/BC_" + utos(i) + "_nodes_" +
 params->prescribed_surfaces_filenames[i].name + "-tet.txt");
// this call will print plain text BC nodes file if the elements are

tetrahedrons (tet4)


if (elements[1][1].how_many_nodes_per_element() == constants::BRICK)
vtk_printer->print_quads_to_vtk_file(
 BC, nodez[1],
 "output/bc/BC_" + utos(i) + "_faces_" + params-
>prescribed_surfaces_filenames[i].name + "-hex.vtk");
// this call will print quadrilateral elements / faces to the
appropriate vtk file
```

Appendix 3 Assessment of the structural integrity of dental materials

This appendix provides support to Section 3.4 and guides assessment of the biomechanical response of mandible materials beyond the conventional stress analysis (which we consider to be essential for further studies on the topic). The three subsections account for three stages of biomaterial failure, from assessment of the risk of fracture occurrence to evaluation of the risk that the carrying material will fail due to the critical crack growth.

Fracture risk analysis

Jaw fracture analysis assumes an assessment if one acts on a mandible with a high impact force (such as a punch [37], a gunshot [53], or a crash [54]) resulting in the generation of stresses exceeding the experimentally determined strength of the carrying material. Because the cortical bone has an anisotropic structure (Table 1), its strength depends on the orientation of osteons to the direction of load [16]. The recommended values of compressive and tensile ultimate strength toward the osteons were σ_{c3} = 199.5 MPa and σ_{t3} = 138 MPa, respectively. The strengths in the plane orthogonal to the osteon axis are approximately the same: compressive strength $\sigma_{c1} = \sigma_{c2}$ = 133 MPa, and tensile strength $\sigma_{t1} = \sigma_{t2}$ = 92 MPa. The shear ultimate strengths in the plane of the orthotropy and without the plane are $\sigma_{23} = \sigma_{13}$ = 79.5 MP and σ_{12} = 53 MPa, respectively. The fracture risk analysis should be conducted using the maximum principal stress criterion (MPSC) [55]. According to the MPSC, it is assumed that failure occurs when the maximum principal stress exceeds the tensile strength σ_T, or when the minimum principal stress is less than the compressive strength σ_C. Thus, the failure index FI is defined as $FI_1 = \sigma_1/\sigma_T$ or $FI_3 = \sigma_3/\sigma_C$, where σ_1, σ_3 are the maximum and minimum principal stresses, respectively. FI is the dimensionless coefficient comparable to 1; when $FI > 1$, failure occurs, and there is a risk of fracture [37]. Generally, zones with FI > 1 can be used for further initiation of cracks and simulation of their propagation.

Fatigue failure analysis

Clinical practice has shown that failures related to dental materials, implants, restorations, and fillings are caused by oral physiological loads [4]. Although the mastication forces are less than the critical breaking forces, they produce damage over long periods, ending with failure. Thus, fatigue analysis aims to investigate how the structure behaves in the long term under smaller physiological forces resulting in stresses lower than the strength of the material [42]. From a biomechanical perspective, cyclic mastication causes cyclic stress changes (Fig. A2), which over time may degrade mechanical properties, initiate and propagate microcracks, and cause fracture, which we defined as ‘‘fatigue failure’’. The fatigue of materials with no preexisting flaws is commonly assessed using the S-N approach and Goodman’s fatigue failure index [56]. $\sigma_{qa}/\sigma_e + \sigma_{qm}/\sigma_u = FFI$, where the endurance strength σ_e and ultimate stress σ_u are experimentally determined material properties of carrying materials (σ_u = 50 MPa and σ_e = 160 MPa for the dentin [56, 57]; σ_u = 106 MPa and σ_e = 140 MPa for the cortical bone [59, 60]). Because the stresses caused by mastication are usually multiaxial with dominant tensile stresses, the equivalent stress theory (EST) is recommended for multiaxial fatigue analysis of materials with ductile behavior [59]. According to the EST, the equivalent nominal stress amplitude can be computed as $\sigma_{qa} = \sqrt{\left[(\sigma_{a1}-\sigma_{a2})^2 + (\sigma_{a2}-\sigma_{a3})^2 + (\sigma_{a3}-\sigma_{a1})^2\right]/2}$, where σ_{ai} and $(i = \overline{1,3})$

are principal alternating nominal stresses $\sigma_{ai} = (\sigma_{\max i} - \sigma_{\min i})/2$. The equivalent nominal mean stress can be calculated as $\sigma_{qm} = \sqrt{\left[(\sigma_{m1} - \sigma_{m2})^2 + (\sigma_{m2} - \sigma_{m3})^2 + (\sigma_{m3} - \sigma_{m1})^2\right]/2}$, where σ_{mi} and $(i = \overline{1,3})$ are principal nominal mean stresses $\sigma_{mi} = (\sigma_{\max i} + \sigma_{\min i})/2$.

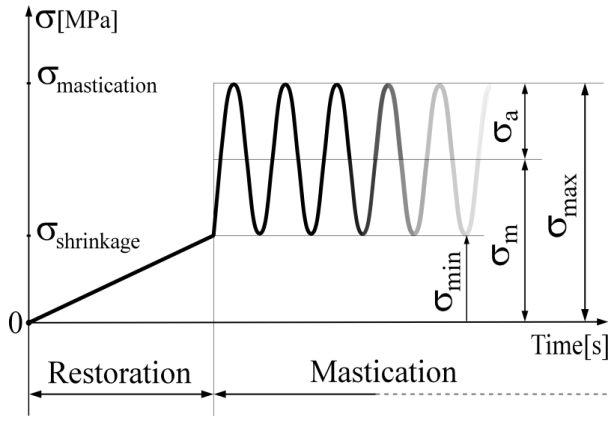

Fig. A2 – Sketch of stress changes caused by restoration/implantation and mastication/exploitation of dental materials.

Fracture Analysis

After the fatigue–failure analysis described in Section 3.4.2, a crack of size a_0 should be initiated in the zone with FFI > 1 to analyze the crack growth and estimate the period of fatigue to fracture. In the literature, fatigue crack growth is commonly assessed using the Paris law: $da/dN = C(\Delta K)^m$ [61, 62, 63] (Fig. A3), where da represents the incremental changes in crack length (Δa); dN represents the number of cycles (ΔN); C and m are the fatigue crack growth coefficient and exponent, respectively; ΔK is the stress intensity range. The stress intensity range is defined as $\Delta K = Y\Delta\sigma(\pi a)^{1/2}$, where Y is a correction factor (1.12 for a shallow flow), $\Delta\sigma$ is the far-field stress range ahead of the crack tip, and a is the crack length. Three distinct phases of the residual fatigue crack growth are shown in Fig. 3 [64]. The subject of study should be the carrying material (dentin or cortical bone) and its period of stable crack growth (region II). More precisely, the aim should be to determine the number of mastication cycles before the failure of the carrying material – the period between the crack initiation (region I) and unstable crack growth (region III). The period of stable crack growth should be at least one million mastication cycles (four years).

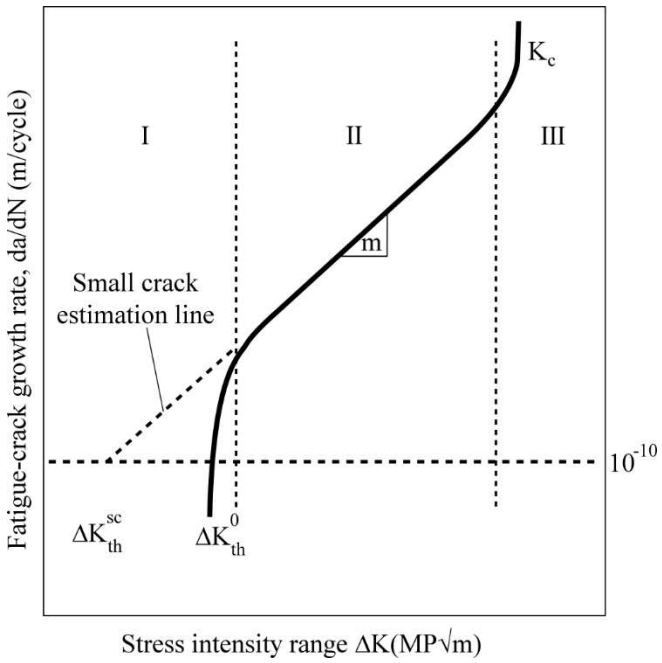

Fig. A3 – Sketch of stress changes caused by restoration/implantation and mastication/exploitation of dental materials.